1.0

28   25

22

20

1.1

1.8

1.25   1.4   1.6

MICROCOPY RESOLUTION TEST CHART

MARTIN MARIETTA

ADA085137

Martin Marietta Laboratories

MML TR 80-19c

THE DELAYED FRACTURE OF ALUMINUM ALLOYS

Prepared by:

J.R. Pickens, D. Venables, and
J.A.S. Green

Prepared for:

DTIC

JUN 4 1980

May 1980

A

80 6 2 038

MML TR 80-19c

THE DELAYED FRACTURE OF ALUMINUM ALLOYS

Prepared by

J.R. Pickens, D. Venables, and J.A.S. Green
Martin Marietta Corporation
Martin Marietta Laboratories
1450 South Rolling Road
Baltimore, Maryland 21227

May 1980

REPORT DOCUMENTATION PAGE	READ INSTRUCTIONS BEFORE COMPLETING FORM

1. REPORT NUMBER	2. GOVT ACCESSION NO.	3. RECIPIENT'S CATALOG NUMBER
MML-TR-80-19c	AD-A085 137	

4. TITLE (and Subtitle)	5. TYPE OF REPORT & PERIOD COVERED
The Delayed Fracture of Aluminum Alloys	Technical Report
	6. PERFORMING ORG. REPORT NUMBER

7. AUTHOR(s)	8. CONTRACT OR GRANT NUMBER(s)
Joseph R. Pickens, Dave Venables, John A.S. Green	N00014-74-C-0277

9. PERFORMING ORGANIZATION NAME AND ADDRESS	10. PROGRAM ELEMENT, PROJECT, TASK AREA & WORK UNIT NUMBERS
Martin Marietta Corporation Martin Marietta Laboratories 1450 South Rolling Rd., Balto., MD 21227	May 80

11. CONTROLLING OFFICE NAME AND ADDRESS	12. REPORT DATE
Department of the Navy Office of Naval Research, Code 471 Arlington, Virginia	5/80
	13. NUMBER OF PAGES
	41
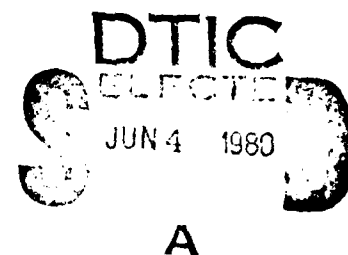
14. MONITORING AGENCY NAME & ADDRESS(if different from Controlling Office)	15. SECURITY CLASS. (of this report)
	Unclassified
	15a. DECLASSIFICATION/DOWNGRADING SCHEDULE

16. DISTRIBUTION STATEMENT (of this Report)

Distribution of this document is unlimited.

17. DISTRIBUTION STATEMENT (of the abstract entered in Block 20, if different from Report)

18. SUPPLEMENTARY NOTES

19. KEY WORDS (Continue on reverse side if necessary and identify by block number)

Stress corrosion cracking, interrupted quenching, oxide film, Auger electron spectroscopy, Auger depth profiling, mud cracking, intergranular fracture, natrual oxide, thermal oxide, aging curves, caustic etch process, Forest Products Laboratory process.

20. ABSTRACT (Continue on reverse side if necessary and identify by block number)

The stress corrosion cracking (SCC) of high purity Al-Zn-Mg alloys has been studied in terms of the effects on SCC susceptibility of: bulk chemistry, bulk microstructure, oxide film chemistry, and oxide film morphology. For alloys having equivalent solute content (wt.% Zn + wt.% Mg), higher bulk concentrations of magnesium lead to slightly increased suscpetibility in acetic-acid-brine solution. Interrupted quenching failed to produce a microstructure exhibiting reduced SCC susceptibility. Preliminary results indicate that an oxide stripping procedure, that removes the magnesium-rich oxide film formed during heat (cont'd)

DD FORM 1473 EDITION OF 1 NOV 65 IS OBSOLETE

Abstract Continued:

treating, and replaces it with an amorphous alumina film, decreases SCC suscept-
ibility.   Porosity in the original castings caused data to be scattered, so new
porosity-free materials have been acquired and the oxide film studies will be
repeated.
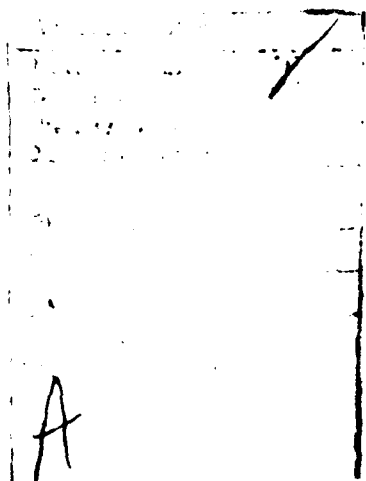
I. INTRODUCTION

A. Summary of Previous Work at Martin Marietta Laboratories

Research in stress-corrosion cracking (SCC) of aluminum base alloys has been ongoing at Martin Marietta Laboratories for 15 years. Initial work concentrated on an improved understanding of the dissolution mechanism of cracking.[1-6] For example, electron microscope examinations of the grain boundary region in Al-Zn-Mg alloys revealed that the rate-limiting step in crack propagation was the stress-assisted dissolution of the solid interspersed between $MgZn_2$ particles along the grain boundary plane.[1] In other work, the velocity of cracking was found to be independent of pH in the range 1 to 6.2 for cracks greater than a certain length.[2] This finding led Laboratories' investigators to believe that a constant pH (~ 3.5) exists near the crack tip.

The effect of alloying additions of recombination "poisons", i.e. As, on Al-Zn-Mg alloys also was studied to see if their retarding effect on the cathodic reaction of the dissolution process would reduce SCC. It was found that certain "poisons" did suppress the cathodic reaction, but the effect of these elements on grain size and precipitate distribution was a greater determinant[3] of SCC behavior.

In the early 1970's, the emphasis of the research switched from understanding the dissolution mechanism to exploring the possible influence of hydrogen embrittlement (HE) on the mechanism of SCC. Green at al.[7] investigated the effect of loading mode on SCC of Al-Zn-Mg alloys, and found that embrittlement in a corrosive solution was greater under Mode I loading than under Mode III loading. They reached the conclusion that HE was operating because Mode I loading has a hydrostatic tensile component,[8] whereas Mode III does not; and, the fugacity of hydrogen in aluminum is greater in a triaxial stress field.[9]

Thus, the greater embrittlement under Mode I than under Mode III loading

is indirect evidence of HE. Furthermore, Green et al.[7] added a recombina-

tion "poison" (As) to the corrosive solution and found that embrittlement

in Mode III decreased, but embrittlement in Mode I increased. They believe

that As retards the recombination of hydrogen, thus maintaining a greater

concentration of monotonic hydrogen in the alloy. This hydrogen, in the

presence of Mode I loading, finds its way to the triaxially-stressed region

at the crack tip,[10] thereby increasing embrittlement. Under Mode III loading,

where there is no triaxial stress field to cause the localized concentration

necessary for embrittlement, the slower dissolution mechanism becomes dominant,

and the retarding effect of As on the cathodic reaction $[H + H \rightarrow H_2 \text{ (gas)}]$

merely suppresses its rate. Numerous other papers in the early 1970's support

the belief that HE can operate in Al-Zn-Mg alloys.[10-19]

With HE considered at least partially responsible for SCC in Al-Zn-Mg

alloys, sophisticated surface science tools, such as Auger electron spectroscopy

(AES), electron spectroscopy for chemical analysis (ESCA), X-ray photoelectron

spectroscopy (XPS), and Auger depth profiling were employed to examine the

composition of the critical grain boundary region. Viswanadham, Green, and

co-workers[20-23] found that the grain boundary was enriched in magnesium in both

the as-quenched, and quenched and aged conditions. This was a surprising

addition to the results of others.[24] Moreover, T.S. Sun, a surface scientist

at the Laboratories, used the plasmon loss energy of the Auger spectra to

determine the binding states of magnesium and zinc in the alloy.[25] These

results are summarized below:

As-quenched condition:

- Free Mg enrichment at grain boundaries
- Free Zn enrichment at grain boundaries

Quenched and overaged condition:

- Virtually all Zn atoms at grain boundaries in MgZn$_2$
- 40% of grain boundary Mg in MgZn$_2$
- 60% of grain boundary Mg existing freely

The fraction of Mg existing freely or in MgZn$_2$ was estimated by comparing the peak-to-peak amplitudes of the Auger spectra.[25] These results showed large Mg concentrations in the region where SCC occurs and led Laboratories investigators to postulate that a magnesium-hydrogen interaction is involved in the SCC mechanism. There is considerable evidence indicating that an interaction between magnesium and hydrogen exists in magnesium-containing, aluminum base alloys.[26-29] Consequently, we have recently sought further evidence of this interaction and, in addition, have studied the composition of the surface film which must be penetrated for SCC to occur.

Auger depth profiling has revealed that the solution treatment temperature has a profound effect on the magnesium concentration of the film.[21-22] This behavior is a result of the competing effects of Mg evaporation at elevated temperature and magnesium oxide formation. Moreover, the solution treatment temperature that results in the highest Mg concentration in the film coincides with the temperature for maximum pre-exposure embrittlement.[16] Unexpectedly, we found that, during storage, aluminum atoms diffuse through the magnesium-enriched film to form additional Al$_2$O$_3$ on the surface.

It is hoped that, ultimately, we can formulate and prove a model by which hydrogen penetrates the film (by interacting with Mg?) and finds its way to the roots of mechanically-induced cracks.

B.   Present Work

In the past year, Dr. Viswanadham initiated work to elucidate the effect of magnesium at the grain boundary and in the bulk on SCC susceptibility of

high-purity Al-Zn-Mg alloys. In his first series of experiments, Dr. Viswanadham studied bulk compositional effects by examining alloys of similar total solute content (wt.% Zn + wt.% Mg) but with various magnesium-to-zinc ratios (wt.% Mg ÷ wt.% Zn; Mg/Zn hereafter). The effect of film composition was intentionally reduced by removing the as-heat-treated oxide film chemically.

In his second series of experiments, interrupted quenching[30] (IQ) was used to modify grain boundary precipitate size and distribution, while similar microstructure was maintained in the bulk of the grains. In this way, the effects of different Mg distributions (free Mg, coarse or fine $MgZn_2$ particles, closely spaced or widely spaced $MgZn_2$, etc.) at the grain boundary could be studied for a constant bulk microstructure.

Dr. Viswanadham resigned from the Laboratories before this work could be completed. His work has been continued by Dr. Joseph R. Pickens, with a renewed emphasis on oxide film studies. In addition, evidence of the Mg-H interaction will be addressed more directly in the coming year.

II. EXPERIMENTAL TECHNIQUES

A. Materials

Four high-purity ternary Al-Zn-Mg alloys were purchased from Metals Specialties Company, Fairfield, Connecticut. They contained two different solute levels (wt.% Zn + wt.% Mg), each with two values of Mg/Zn. The compositions of the alloys are listed in Table I; total impurity content was less than 0.01 wt.%. These alloys were used in the three major experiments: effects on SCC of bulk composition, interrupted quenching, and oxide film type.

TABLE I

Alloy Composition

Element	Alloy A (wt.%)	Alloy B (wt.%)	Alloy C (wt.%)	Alloy D (wt.%)
Mg	2.5	3.7	2.6	4.0
Zn	5.3	4.4	7.7	6.4
Cu	<.01	<.01	<.01	<.01
Cr	<.01	<.01	<.01	<.01
Si	<.01	<.01	<.01	<.01
Ni	<.01	<.01	<.01	<.01
Mn	<.01	<.01	<.01	<.01
Fe	<.01	<.01	<.01	<.01
Ti	<.01	<.01	<.01	<.01
Solute content (wt.% Mg + wt.% Zn)	7.8	8.1	10.3	10.4
Mg/Zn[a]	.47	.84	.34	.63

[a] wt.% Mg $\div$ wt.% Zn.

B.   Procedure

1. Effect of Bulk Composition

Sheet tensile specimens $3 \times 0.5 \times 0.04$ in. were machined from each of alloys A, B, C, and D. Aging curves were developed, and specimens were aged to peak hardness. The as-heat-treated oxide films were removed by the following procedure:

a. Washing in acetone
b. Pickling in 50 g HNO_3/liter for 1 hr at $30 \pm 2°C$
c. Rinsing in distilled water
d. Etching in 100 g NaOH/liter solution for 1 min at $65 \pm 1°C$
e. Rinsing in distilled water
f. Removing dark Zn deposit and neutralizing for 1 min in solution as in (b)
g. Rinsing in distilled water
h. Washing in acetone
i. Drying at room temperature for 5 min
j. Storing in a silica gel desiccator for 24 to 48 hr

The oxide surfaces were examined by AES. Specimens were then tested in tension at room temperature in a solution of 30 g NaCl + 80 ml 0.5N CH_3COONa + 20 ml 0.5N CH_3COOH (pH ~ 5.1). Stress vs life-to-failure curves were constructed.

2. Interrupted Quenching Experiments

Alloys A and B were used for this experiment. Three groups of machined tensile specimens from each of the two alloys were solution heat treated at 475°C for 2 hr, subjected to an interrupted quench in a 200°C oil bath for 0, 30, and 60 min, and then quenched in ice water. Aging curves were developed, and each group of specimens was aged to the same hardness (which was close to peak hardness for each ternary alloy).

Stress-life data were generated in the aforementioned acetic acid-brine solution. TEM foils were then made to characterize the microstructures.

3. Natural vs Thermal Oxides

A stripping procedure to remove the magnesium-enriched oxide film was developed. Sheet tensile specimens of alloy B were solution treated at 475°C, quenched in ice water, and then aged to peak hardness, using the previously-determined aging curves as a guide. Half of the specimens had the thermal film (i.e., as-heat-treated) and were tested in tension in acetic acid-brine. The other half were tensile tested in the same solution but after the thermal film was removed and a "natural" oxide film had been allowed to form at room temperature. Stress-life plots were made, and Auger depth profiling was used to determine the magnesium profile in each film of the alloy. Ultra-high resolution scanning electron microscopy (URSEM) was used to characterize the oxide morphology of the thermal and natural oxide films.

Fracture surfaces were examined, with much work concentrating on methods of removing the corrosion product from the fracture surfaces.

III. RESULTS AND DISCUSSION

A. Results of Bulk Composition Experiment

The aging curves developed are shown in Figs. 1-2. Each of the four alloys was aged to peak hardness (see Table II). Stress vs life-to-failure data are plotted in Fig. 3.

The two higher solute-containing alloys (C and D) showed less SCC resistance than did the lower solute alloys A and B. Moreover, at both solute contents, the alloy having lower Mg/Zn showed greater SCC resistance. However, the differences in SCC resistance were not marked.
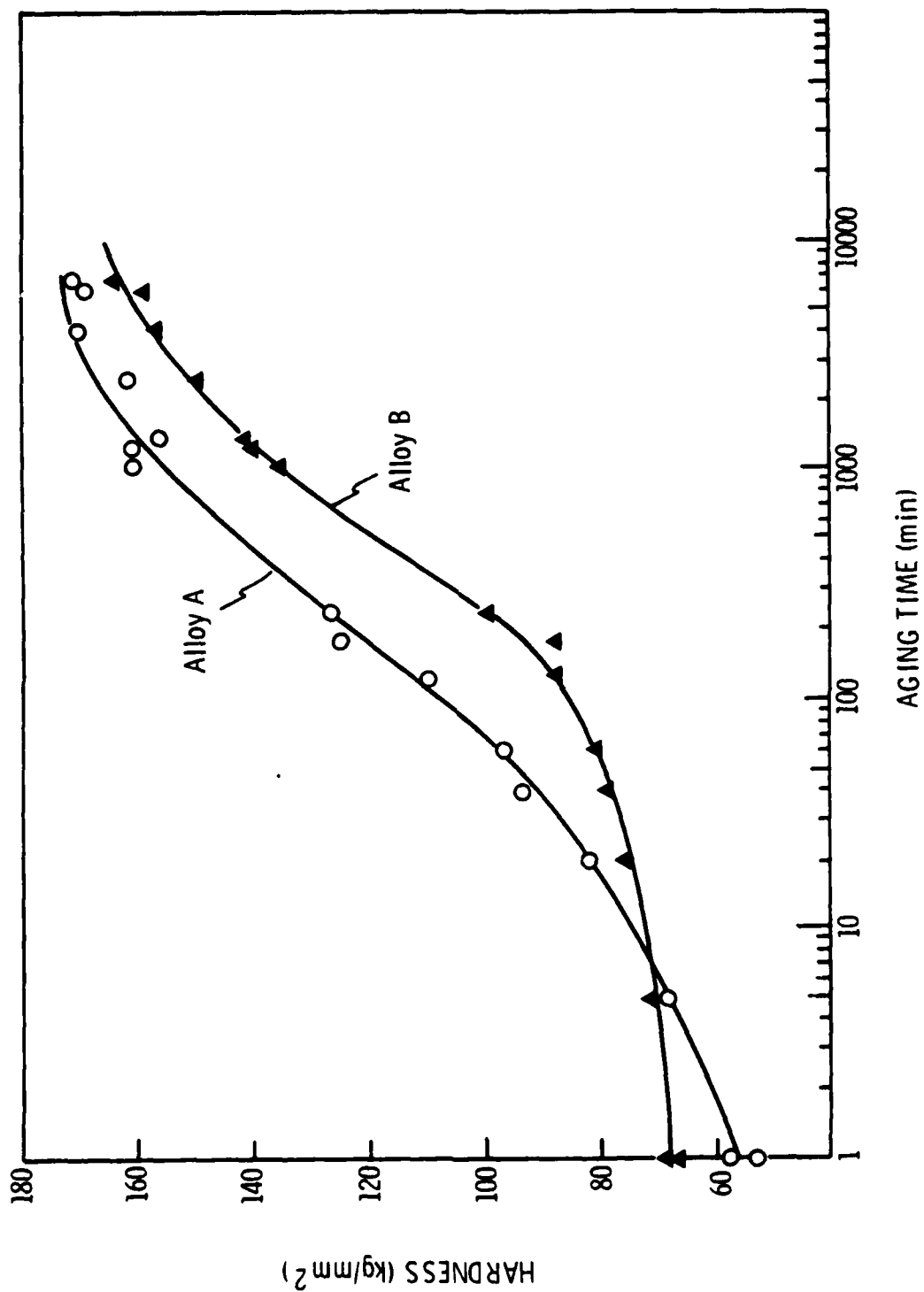
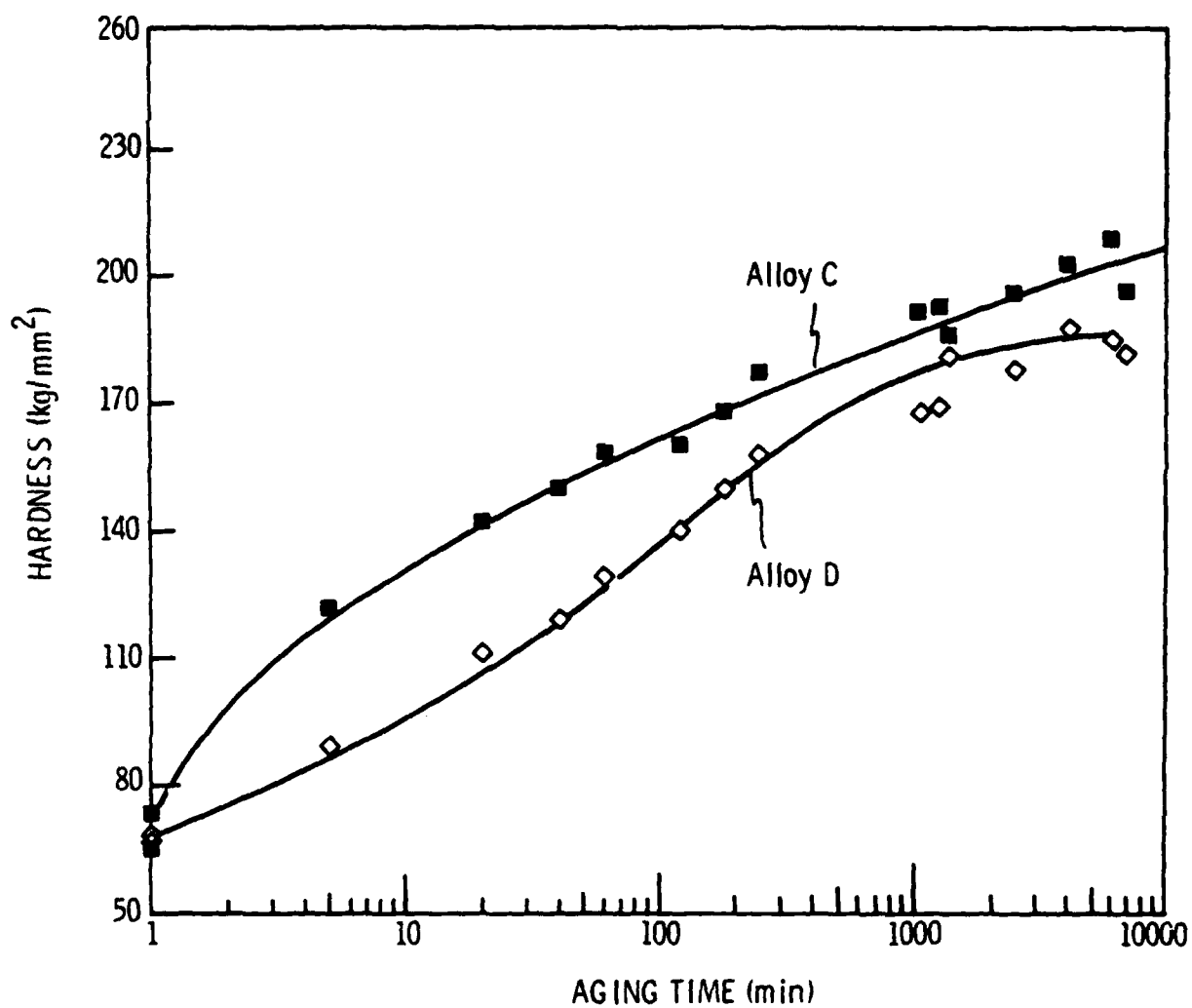Figure 1. Aging curve for alloys A and B.
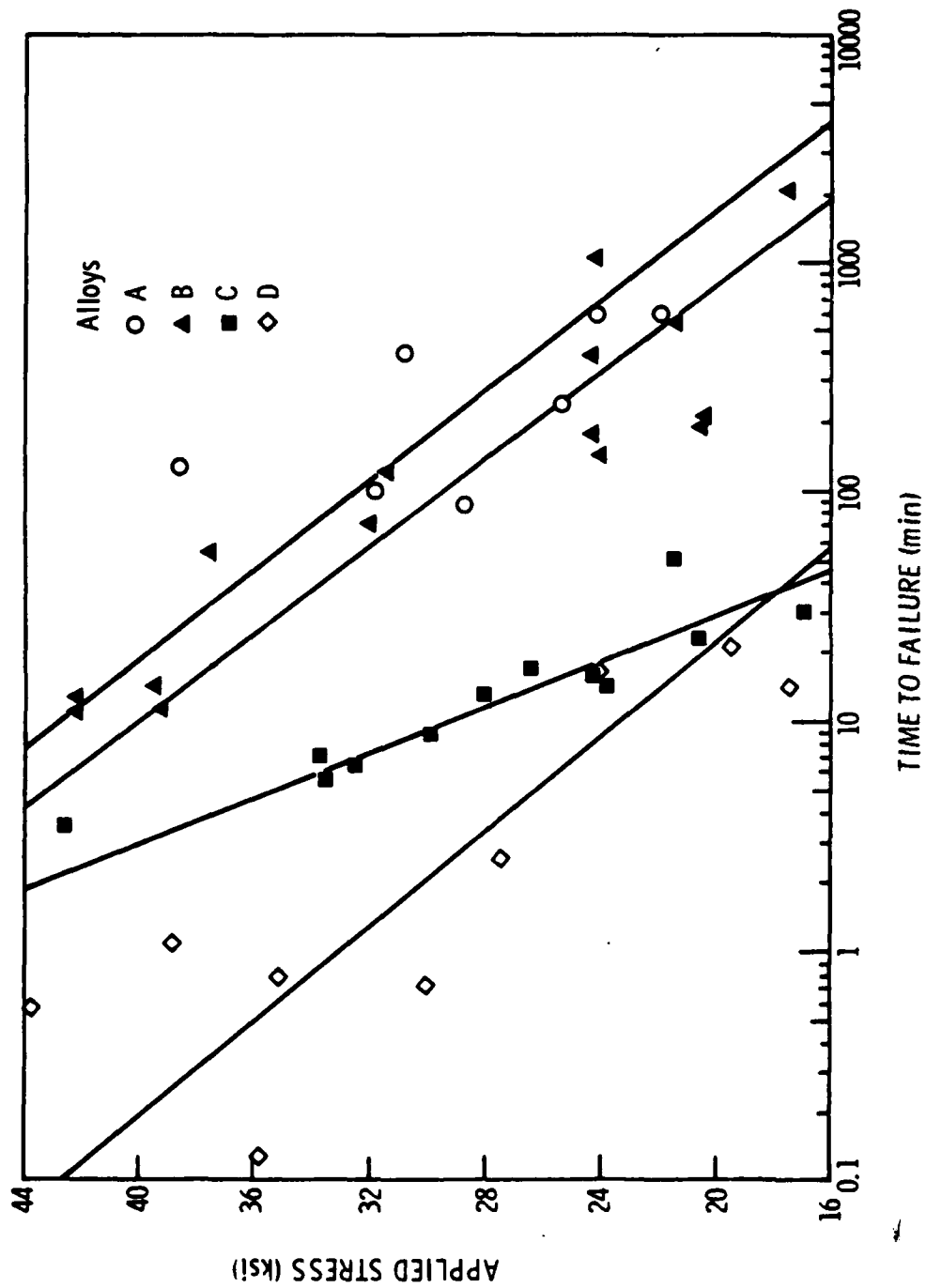
Figure 2. Aging curves for alloys C and D.

Figure 3. Stress vs life-to-failure in acetic acid-brine for alloys A, B, C, and D.

TABLE II

Hardness of Bulk Composition Specimens

Alloy	Mean Vickers Hardness (kg/mm^2)	Standard Deviation
A	150	4
B	156	3
C	147	5
D	159	1

Since the higher values of Mg/Zn reduced SCC resistance, these results somewhat support our contention that a Mg-H interaction is involved in the SCC of Al-Zn-Mg alloys. The effect is not dramatic because differences in composition in the critical film region are slight. Figures 4-7 show the Auger depth profiles of the surface regions of alloys A, B, C, and D, respectively, after the thermal oxide films were stripped off and before testing in corrosive solution. As can be seen, the magnesium content in the surface region of all four alloys appears to be negligible. The Mg content near the surface of alloy C appears to be slightly higher; however, since this trace represents five times the Mg Auger signal, the amount is still negligible. Figure 8 shows, for comparison, the high magnesium content in the film region of alloy B having a thermal (as-heat-treated) oxide film.

It should be noted that the Zn and Na curves coincide because their Auger electrons are at the same energy. The Na is most probably contamination from the oxide stripping procedure which uses NaOH. Since the sodium content is expected to decrease rapidly with sputtering, any counts subsequently detected are from Zn. After the sodium content decreases, the Zn profiles in A and B look quite similar, as do those in C and D.

The specimens used for the depth profiling were previously fractured in air to establish their yield strengths (material was limited). The high carbon content on all surfaces was probably caused by small cracks in the surface absorbing acetone used in the degassing process before Auger depth profiling. It is not surprising that total bulk solute content (wt.% Mg + wt.% Zn) has a noticeable adverse effect on SCC resistance. However, the slight adverse effect of higher bulk Mg/Zn on SCC resistance suggests that SCC resistance can be enhanced by higher Zn additions (and lower Mg additions) at a given solute level.
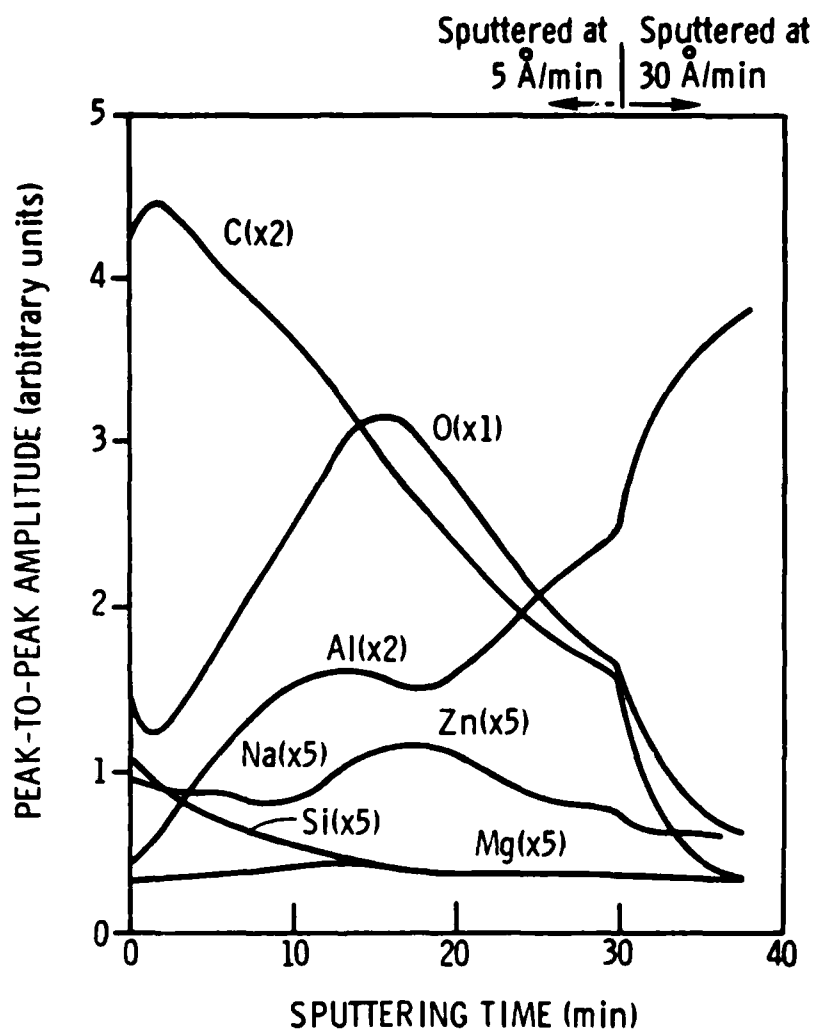
Figure 4. Auger depth profile of room temperature-formed oxide on alloy A.
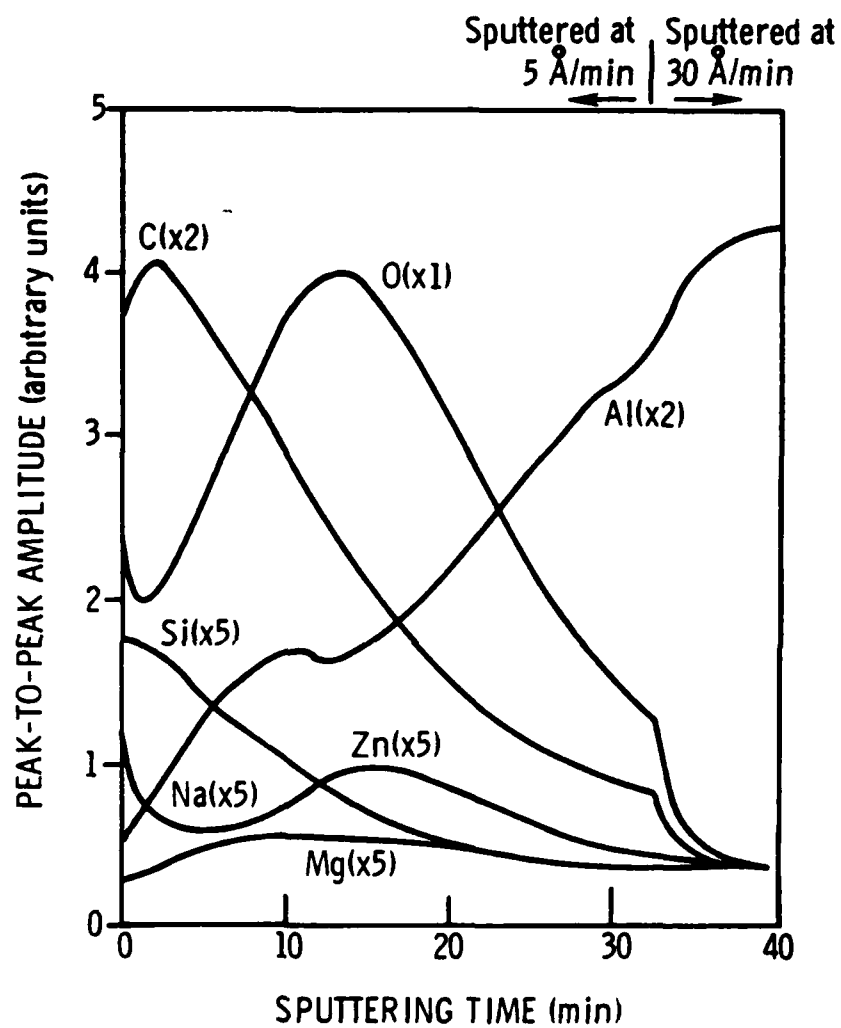(Note that Na and Zn are at the same energy.)

Figure 5. Auger depth profile of room temperature-formed oxide on alloy B. (Note that Na and Zn are at the same energy.)
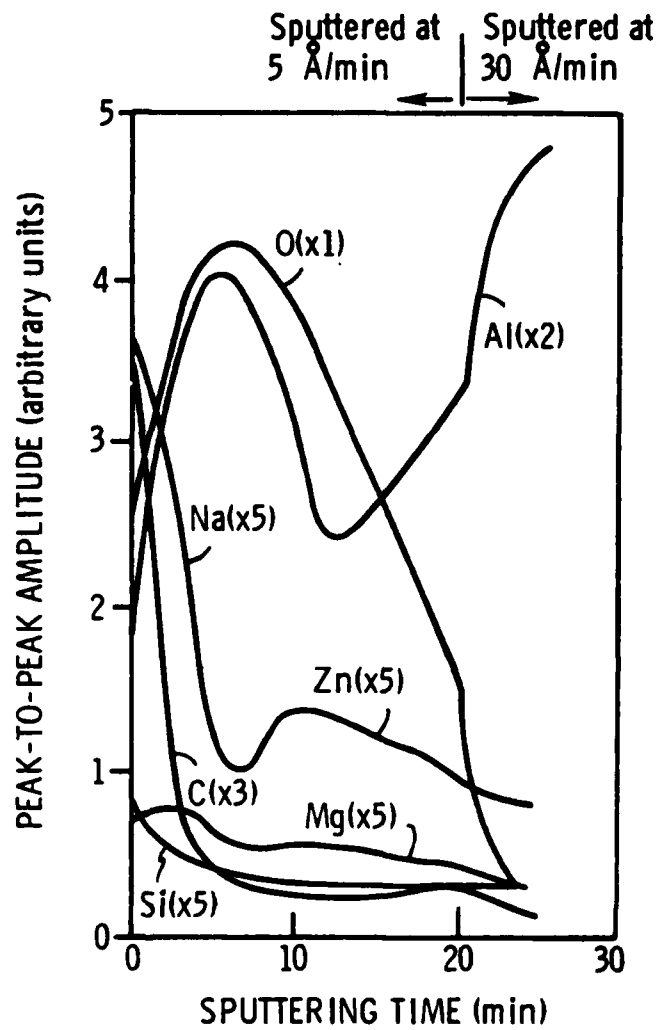
Figure 6. Auger depth profile of room temperature-formed oxide on alloy C. (Note that Na and Zn are at the same energy.)
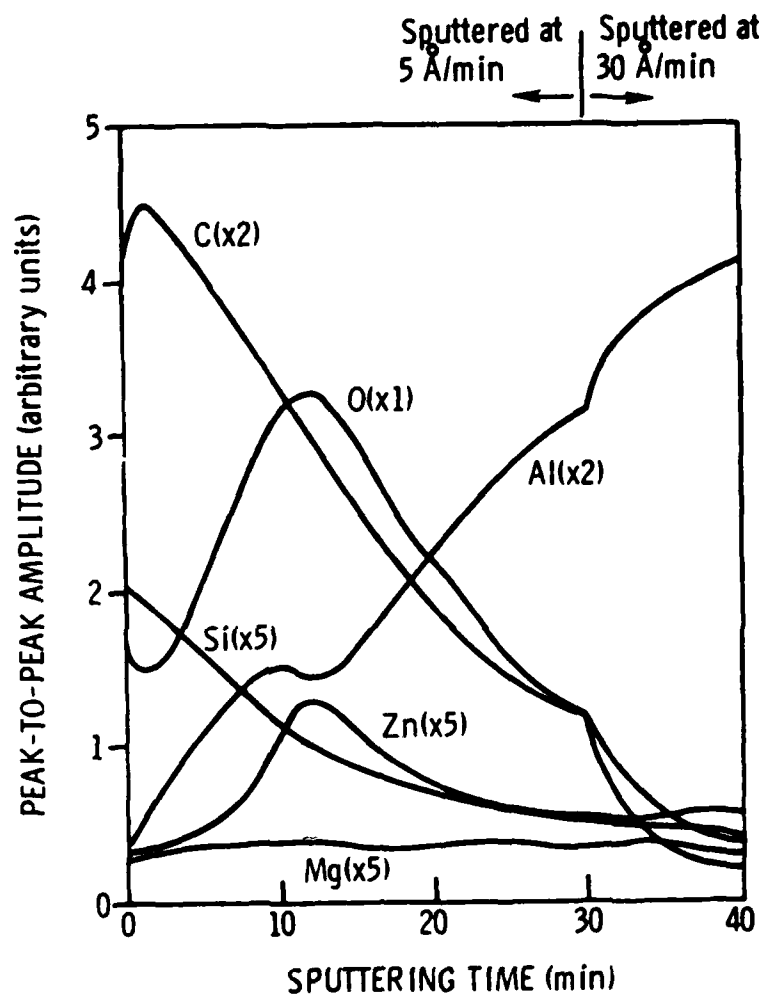
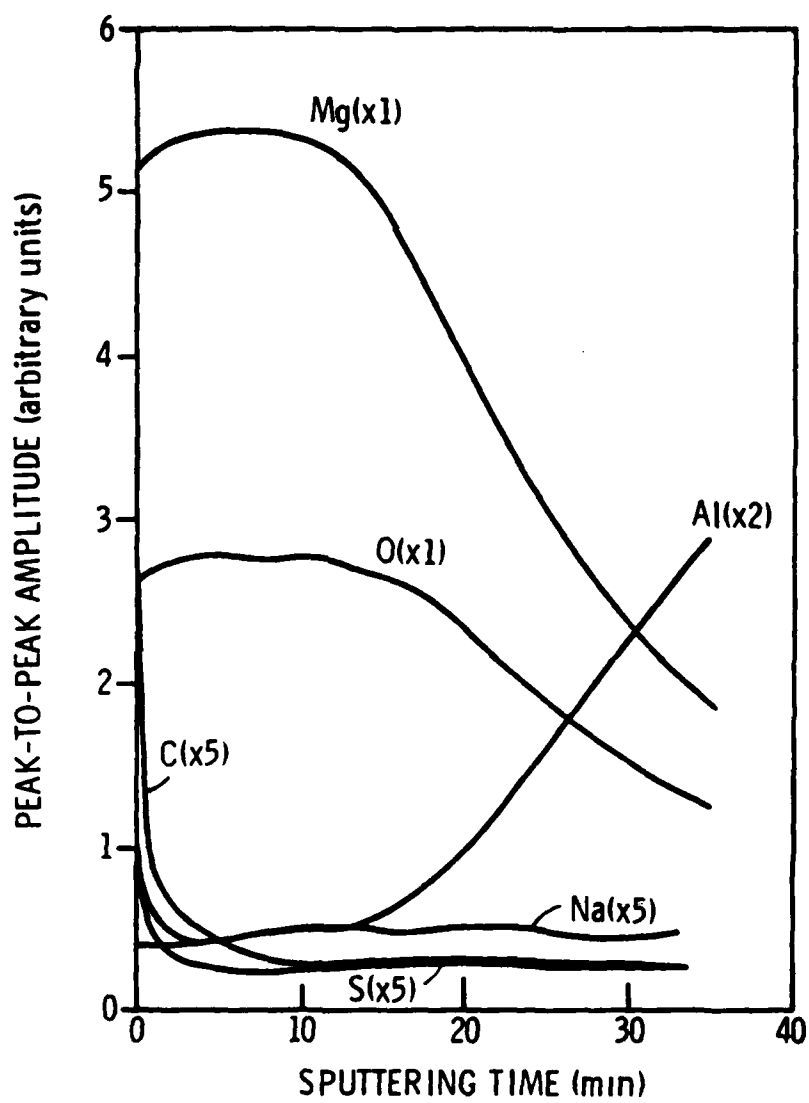Figure 7. Auger depth profile of room temperature-formed oxide on alloy D.

Figure 8. Auger depth profile of thermal oxide on alloy B. Sputtered at ~ 30 Å/sec.

The large scatter in the data can be explained by the significant porosity in the ingots of the alloys made by Metals Specialties Co. (see Fig. 9),which were subsequently rolled. In addition, alloys of a given total solute content could not be aged to precisely the same hardness level.

B.   Interrupted Quenching Experiments

Aging curves developed for the three IQ times for each of alloys A and B are shown in Figs. 10 and 11. Alloys were aged to similar, but not identical, hardness levels (see Table III). Stress-life curves are shown in Fig. 12.

The scatter in the stress-life data is too great to allow firm conclusions. SCC resistance appears to be lowest for water-quenched specimens (0 IQ time), greater for 60-min IQ, and even greater for 30-min IQ as seen in Fig. 12. The scatter is probably due to 1) porosity in the starting material, and 2) our inability to age to identical hardness values.

IQ time did not appear to have a dramatic effect on SCC resistance, which is consistent with our earlier findings using different IQ parameters.[31] In addition, the difficulty in limiting the data scatter has caused us to discontinue this experiment. Studies of the oxide film composition appear to have greater potential for producing meaningful results.

C.   Natural vs Thermal Oxides

Considerable effort was expended in developing an oxide stripping procedure that could remove the magnesium-rich, heat-treated (thermal) oxide film, thereby allowing an amorphous alumina film to form in its place. The Pourbaix diagram for aluminum (Fig. 13) suggests that a pH < 3.5 or > 9 is necessary to remove alumina and the Pourbaix diagram for magnesium (Fig. 14) shows that a pH < 11 is necessary to remove magnesia from each material's
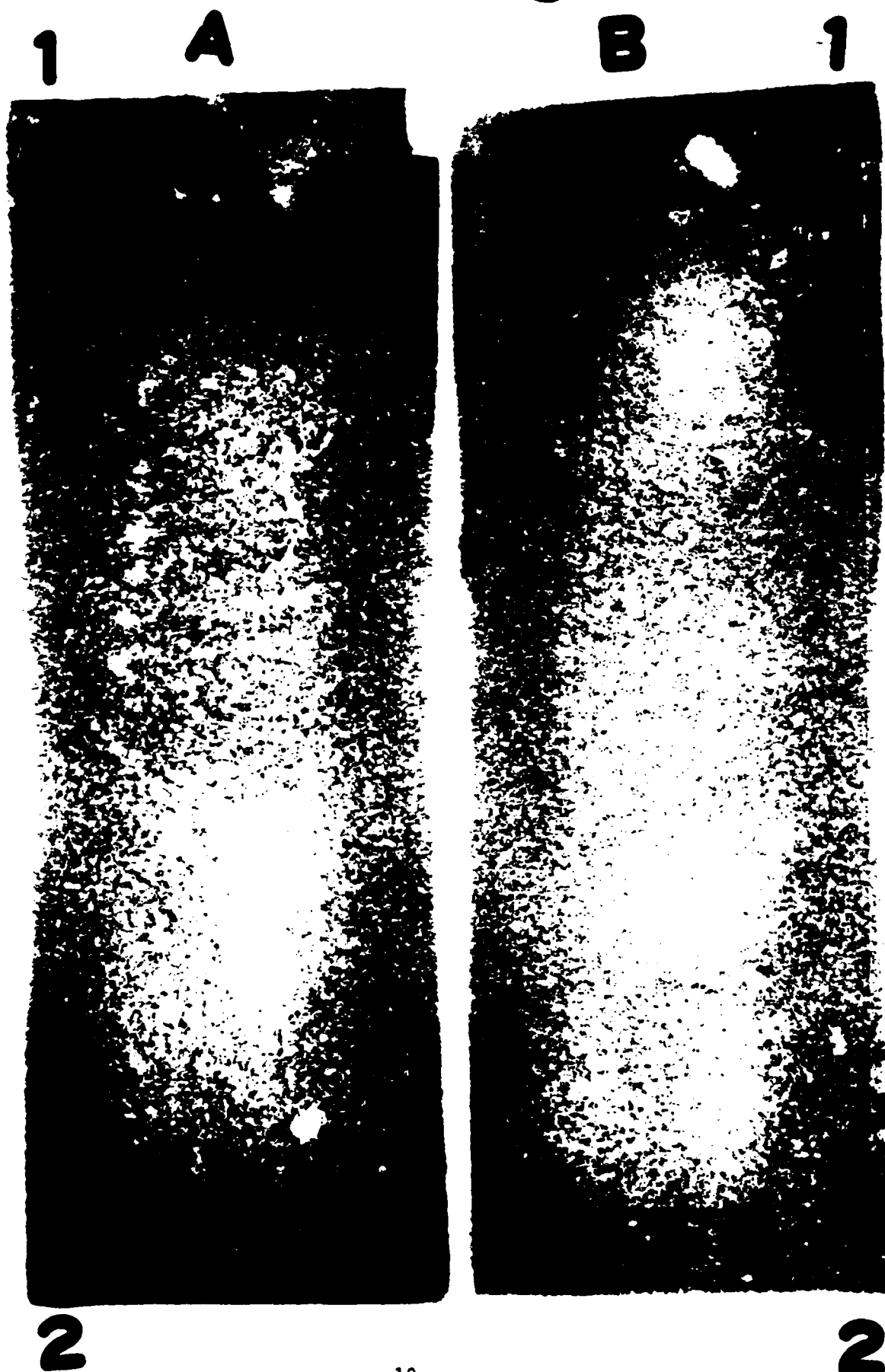
-18-

4 26 79

Figure 9. X-ray photograph of ingots of alloys A and B showing porosity.
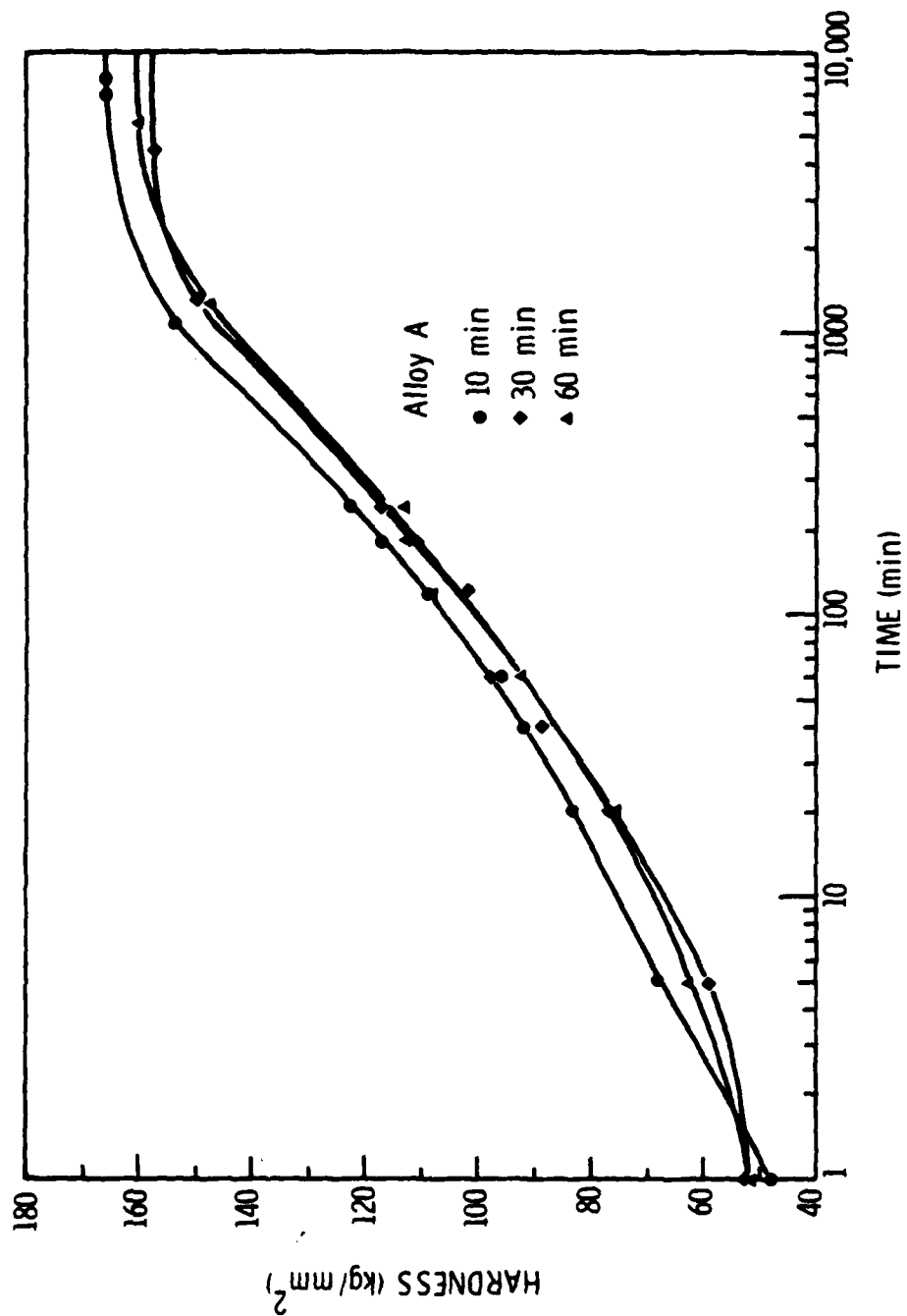
-19-

Figure 10. Hardness vs aging time curves for alloy A aged at 120°C. The alloy was solution treated at 475°C for 2 hr and the quench was interrupted at 200°C for 10, 30, and 60 min.
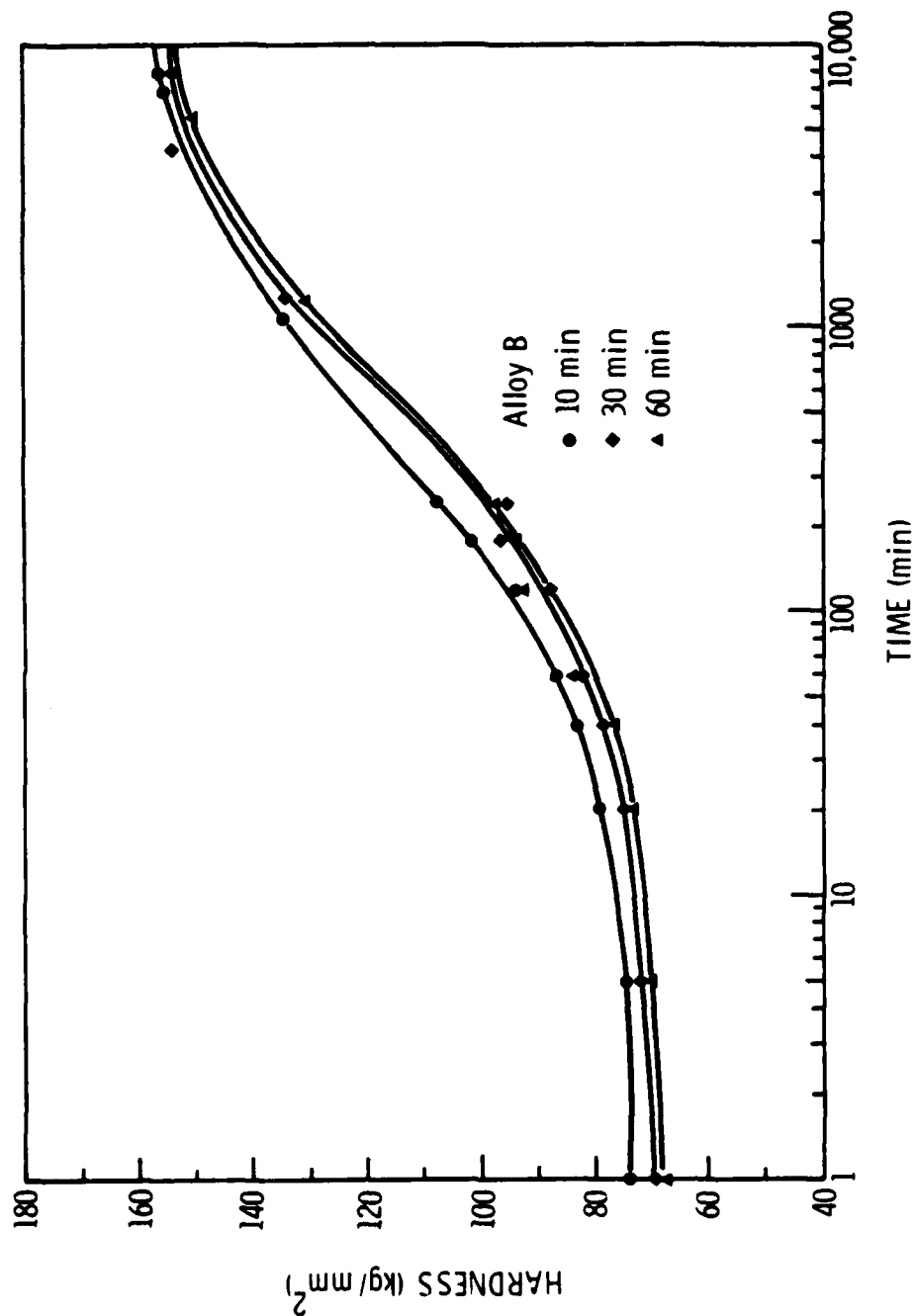
Figure 11. Hardness vs aging time curves for alloy B aged at 120°C after quench interruption at 200°C for 10, 30, and 60 min.

TABLE III

Hardness of Interrupted Quench Specimens

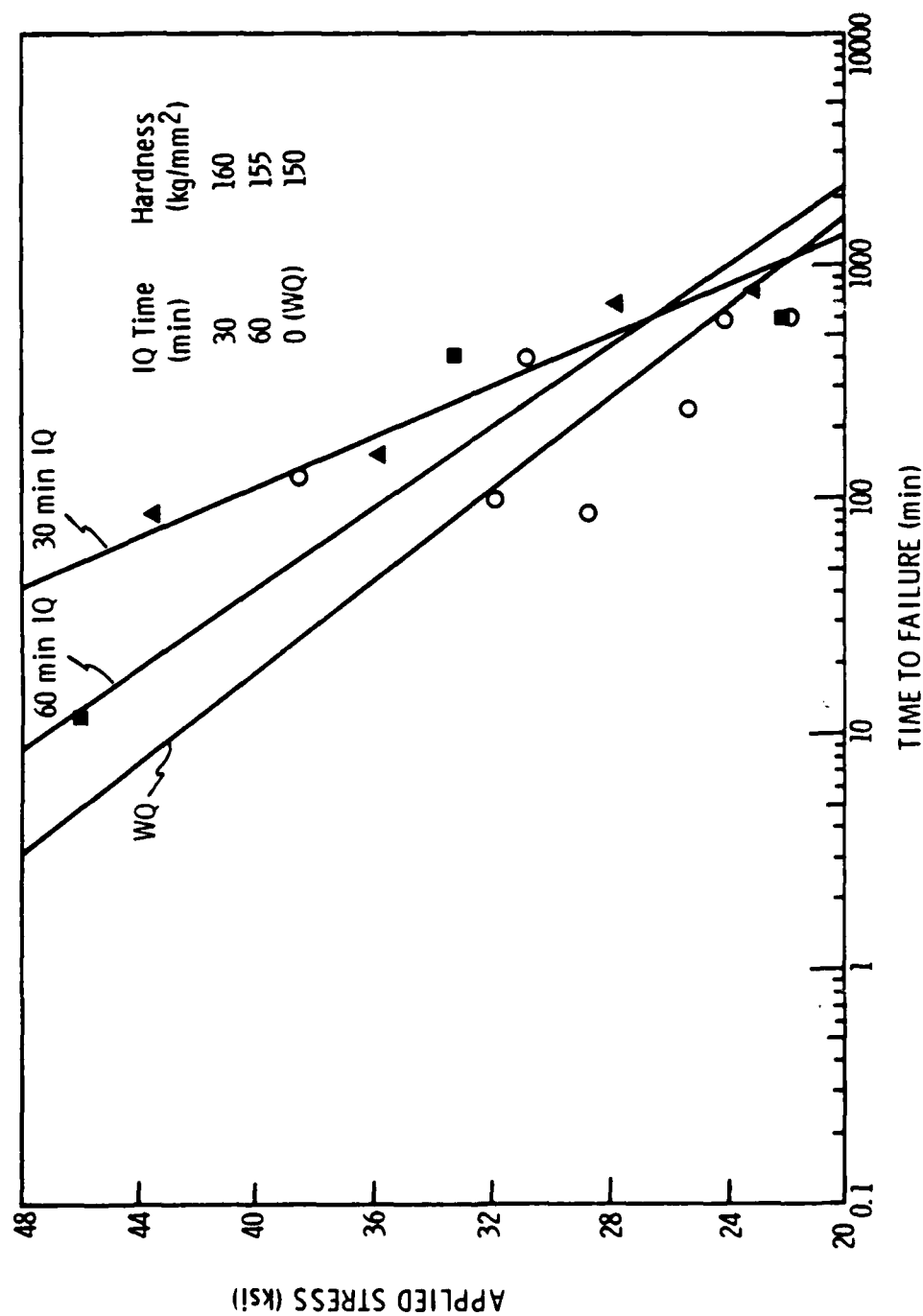| Alloy	Interrupted Quench Time (min)	Mean Vickers Hardness (kg/mm^2)	Standard Deviation
A	0	150	4
A	30	160	5
A	60	155	6

Figure 12. Stress vs time-to-failure of alloy A; interrupted quench tests. (Heat treated 475°C, 2 hr, IQ in 200°C oil bath, aged at 120°C to peak hardness.)
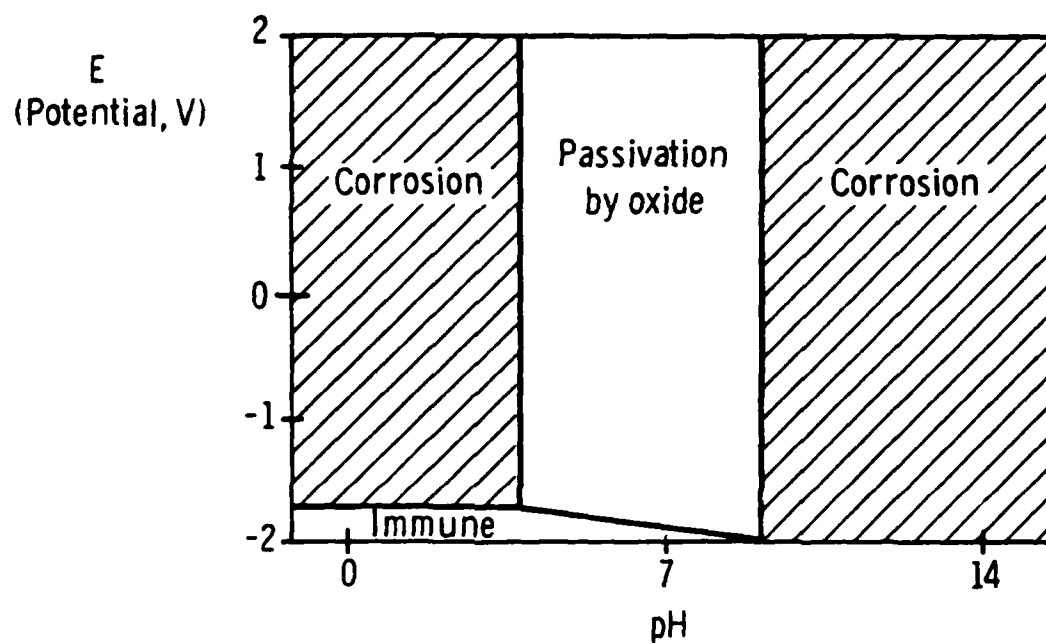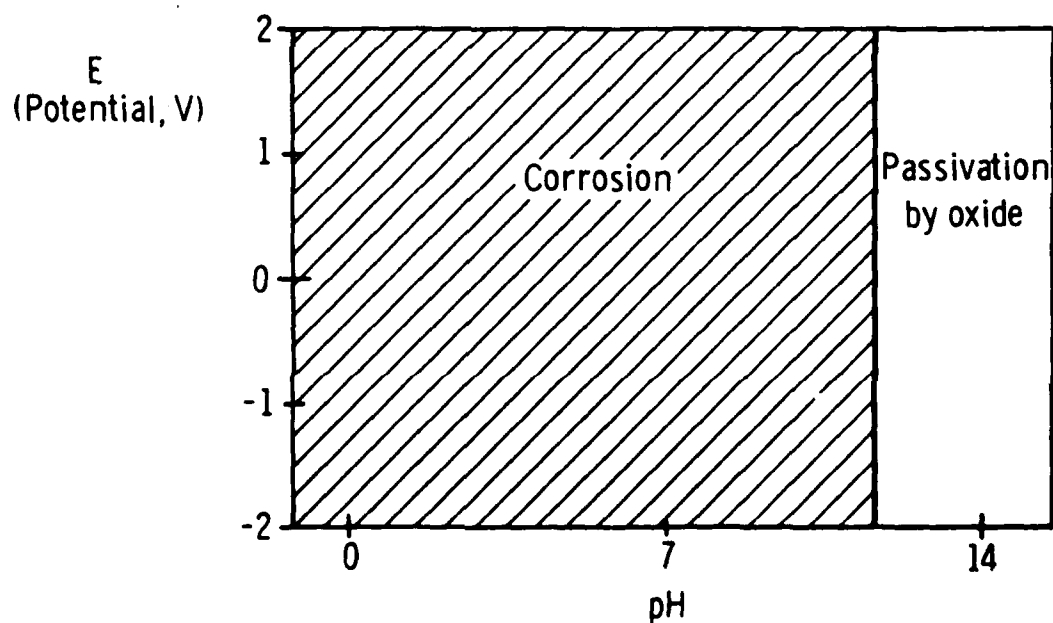
Figure 13. Pourbaix diagram for aluminum.

Figure 14. Pourbaix diagram for magnesium.

surface. Using these pH considerations as a rough guide, the following etching procedures were investigated.

1. Caustic Etch Process (CE)[32]

Specimens were cleaned ultrasonically in acetone and were immersed in 1N NaOH solution (pH ~ 13.3) for 20 min at room temperature, rinsed in distilled water, immersed in 10% HNO_3 (by volume; pH ~ 1.0) for 1 min, rinsed in distilled water, and then placed under vacuum (~ 700 torr) in a desiccator for ~ 35 min.

The caustic etch process is basically the procedure described in the Metals Handbook[32] for preparing aluminum surfaces for macroscopic examination. However, some modifications were made in the procedure based on a study of the effects of immersion time, solution concentration, and solution pH on the specimen surface (e.g., the HNO_3 concentration was lowered to avoid uneven pitting, etc.). In addition, the specimens were placed under vacuum immediately after etching to try to prevent formation of undesirable hydration products.

Auger depth profiles of the CE surface indicated that the oxide film was 25 Å and the profiles, in conjunction with XPS studies (Fig. 15) indicate that the oxide consisted of Al and O with only trace amounts of Mg. Furthermore, a subsequent URSEM examination of the surface (Fig. 16) did not reveal the characteristic "cornflake" morphology[34] of crystalline hydration products, indicating that our vacuum technique was effective in preventing hydration. This examination also indicated that the film was nonporous and relatively thin. Hence, the CE process effectively removed the thermal oxide film and replaced it with a 25 Å-thick, nonporous, amorphous Al_2O_3 layer.
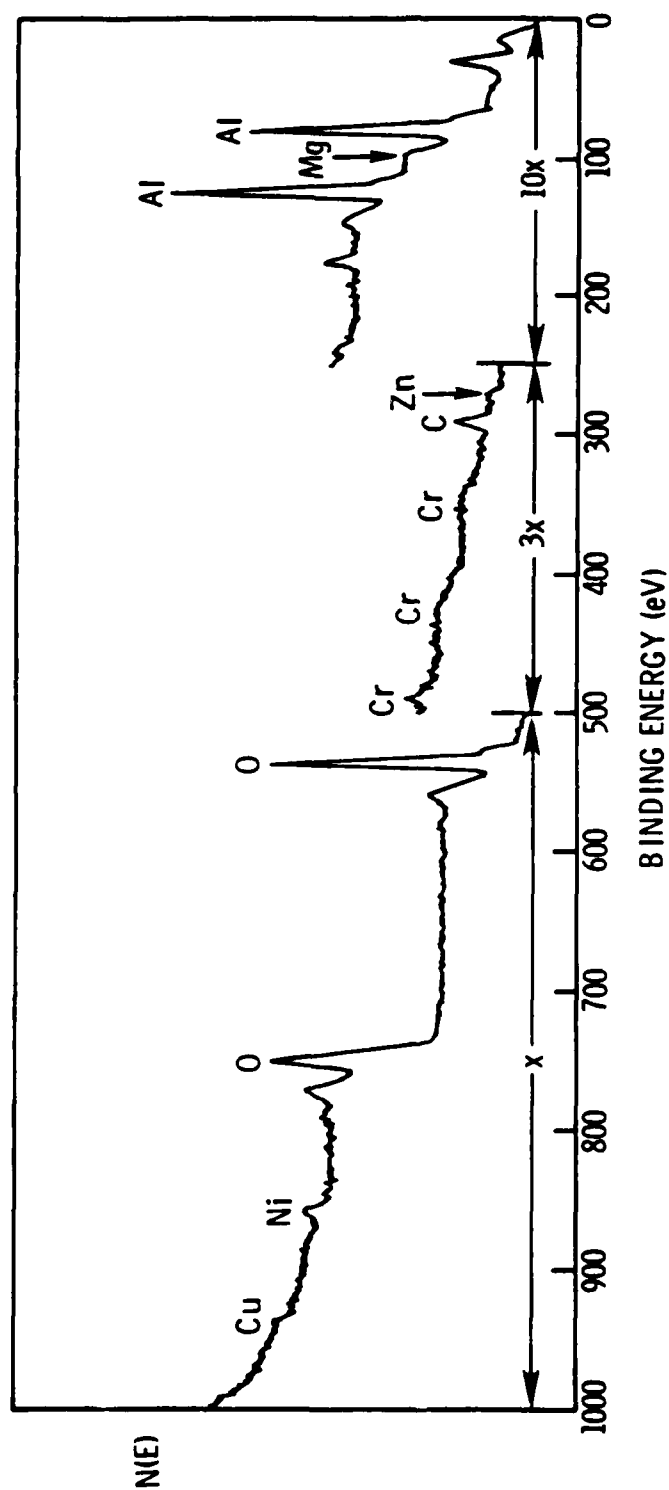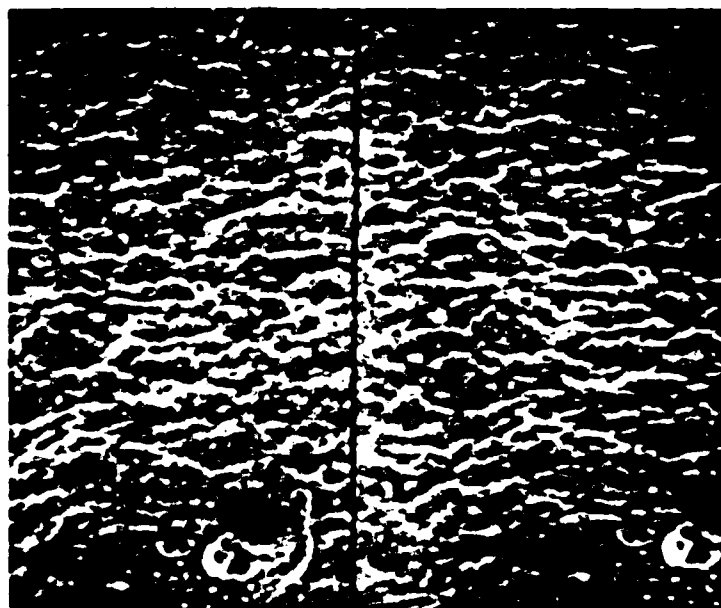
Figure 15. XPS scan of natural oxide film of alloy B.

50,000x

Figure 16.   URSEM photomicrograph of natural oxide of alloy B.

2. Forest Products Laboratory Process (FPL)[33]

Following ultrasonic cleaning in acetone, the specimens were immersed for 10 min in a solution containing $Na_2Cr_2O_7 \cdot 2H_2O$, H_2SO_4, and H_2O in a 1:10:30 weight ratio at 68°C.

The FPL process is used commercially to prepare aluminum surfaces for adhesive bonding by stripping off pre-existing oxide layers and replacing them with a 200-400 Å-thick, slightly porous Al_2O_3 layer.[35] It was not known, however, whether this process effectively removed MgO. This question was resolved with the aid of an XPS scan of the FPL surface (Fig. 17), which indicated that no Mg was present on the FPL surface, i.e., the FPL process effectively removes the thermal oxide film and replaces it with a thick, slightly porous, Al_2O_3 film.[35]

In other words, both the CE and FPL processes remove the thermal oxide layer and replace it with an Al_2O_3 layer. However, the nonporous nature of the CE film led us to select the caustic etch process for forming our "natural" oxide film and evaluating its role in stress corrosion.

3. SCC Resistance of Alloys with Natural and Thermal Oxide Films

The stress vs life-to-failure data for alloy B with the "thermal" (Mg-rich) and "natural" (amorphous alumina) films are shown in Fig. 18. Although the data contain significant scatter, the natural film may appear to enhance SCC resistance. Thus, with a simple etching procedure, we may be able to increase the SCC resistance of Al-Zn-Mg high-purity ternary alloys and perhaps that of commercial 7xxx alloys. This experiment will be repeated on new, high-purity Al-Zn-Mg alloys now being made up by Reynolds Metals Co. (Richmond, VA).

The oxide stripping procedure will be tried on purchased commercial 7075 0.050-in. sheet to investigate its effect on the SCC resistance of commercial 7xxx alloys. Alloy 7075 contains a grain refiner that inhibits
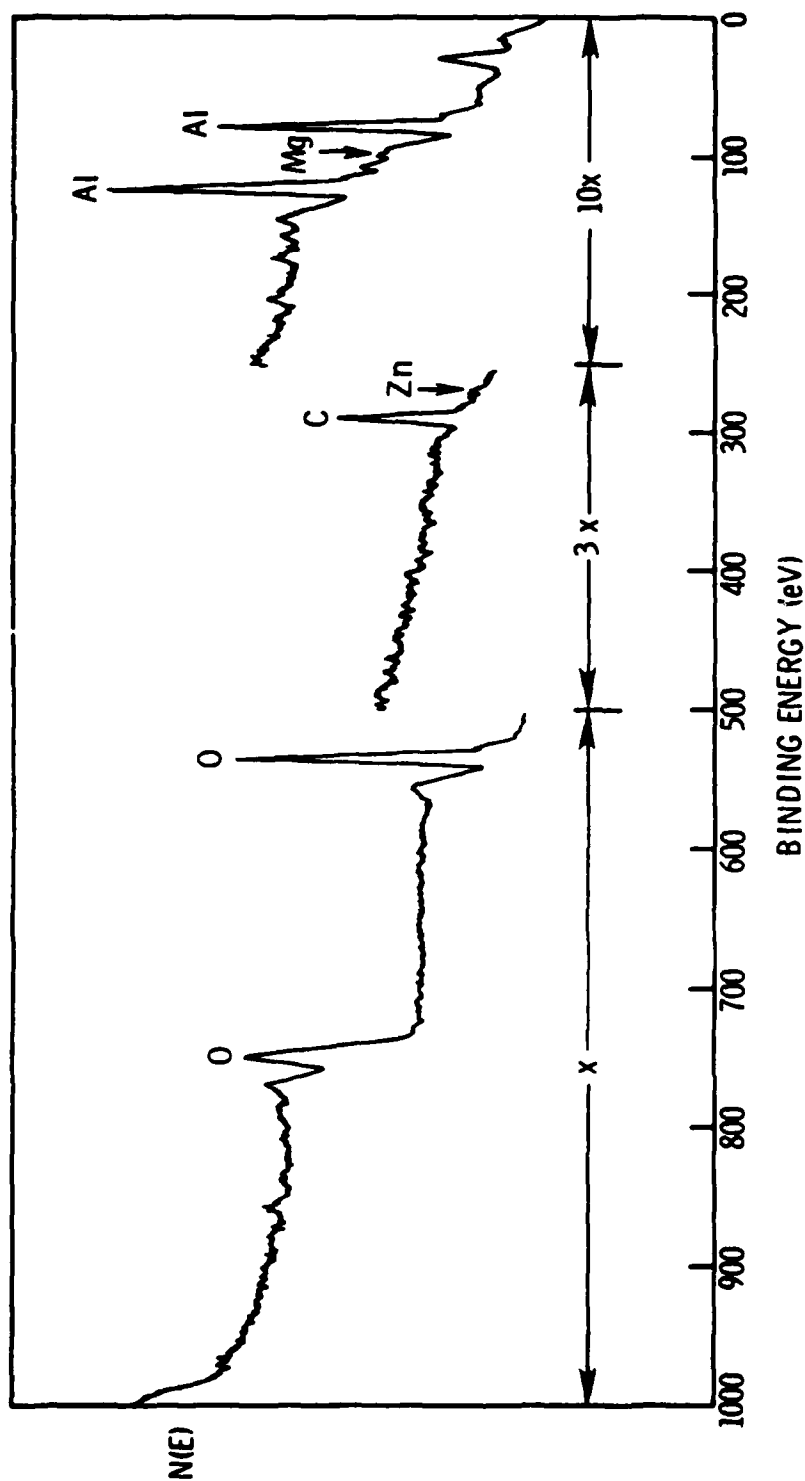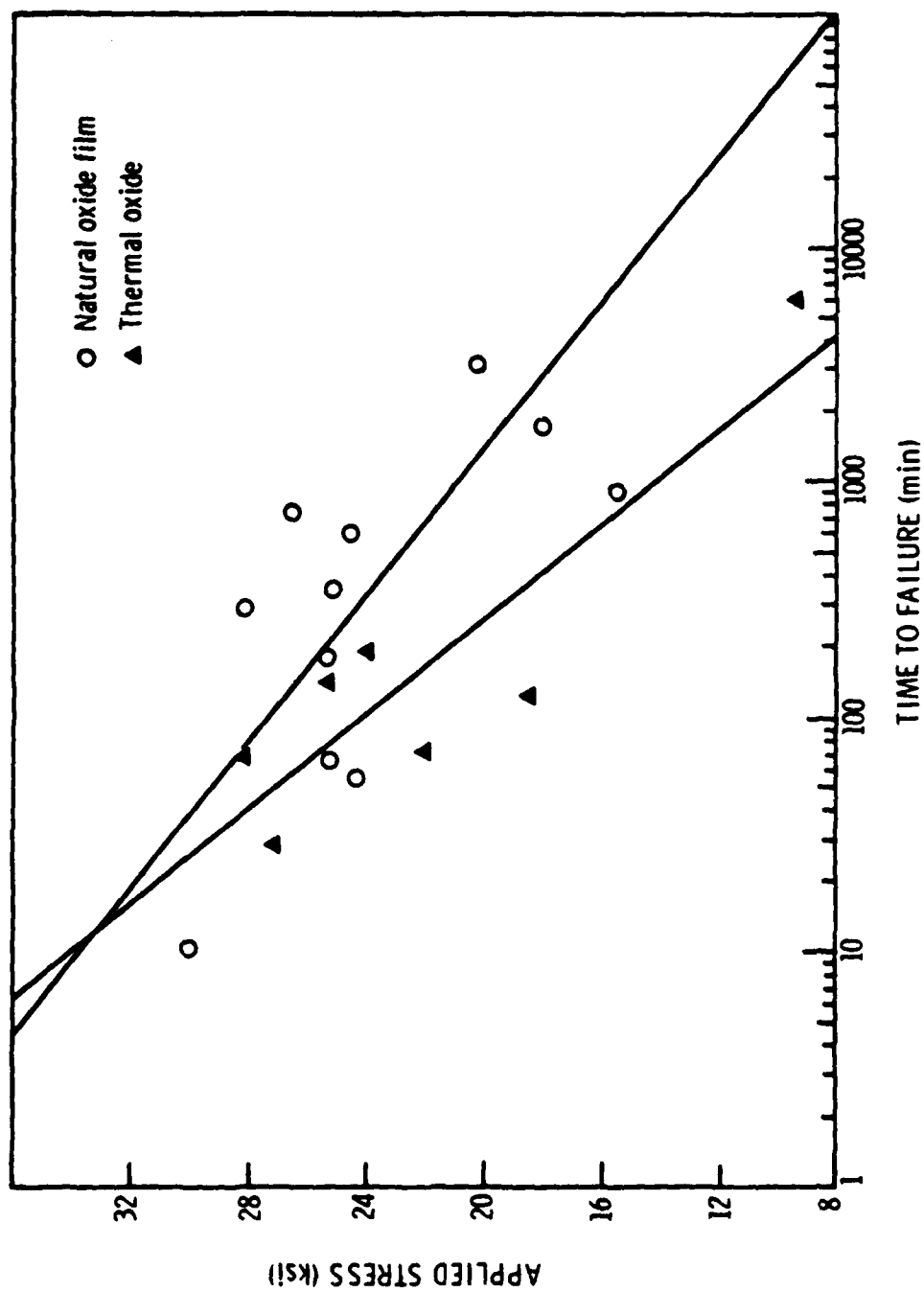
-28-

Figure 17. XPS scan of FPL surface.

Figure 18. Stress vs time-to-failure for alloy B comparing behavior of natural thermal oxide films.

recrystallization. Therefore, the alloy is not susceptible to SCC in the longitudinal direction and is only slightly susceptible in the long transverse direction of this thin sheet. Unsuccessful attempts have been made to recrystallize the 7075 to an equiaxed grain structure that will be susceptible to SCC in the longitudinal or transverse direction. (Obviously, tensile specimens must be machined in either the longitudinal or long transverse direction.)

The natural and thermal oxide films of alloy B were also studied on the URSEM. The thermal oxide appears to be thick, with numerous fine pores on the surface (see Fig. 19). Particles of Ni-Fe-Zn-Mg and Cu-Ni-Fe also appear on the surface. These contaminant particles may be crystalline and appear to grow out of the surface from grain boundaries. The natural oxide (Fig. 16) is featureless, as would be expected for an amorphous oxide.

Auger depth profiles of the thermal and natural oxide surfaces (Figs. 8 and 20) were made to 1) show that the oxide stripping procedure was successful in removing magnesium, 2) estimate the differences in magnesium content of the two films, and 3) estimate the thickness of the oxides. As can be seen by comparing the figures, the natural oxide film is virtually magnesium-free, and the thermal oxide film is enriched in magnesium. The thermal oxide film is fairly thick (900 Å), while the natural oxide film is quite thin (25 Å). Despite this difference, the natural oxide film appears to afford the alloy greater protection from SCC.

4. Fracture Surfaces in Alloys with Thermal and Natural Oxide Films

Fractographic studies initiated on specimens of alloy B (thermal and natural films) showed that the corrosion product on the fracture surface could not be easily removed. Figure 21 shows the "mud cracking"[21] corrosion product on the fracture surface. B.F. Brown[36] has shown that the mud cracking
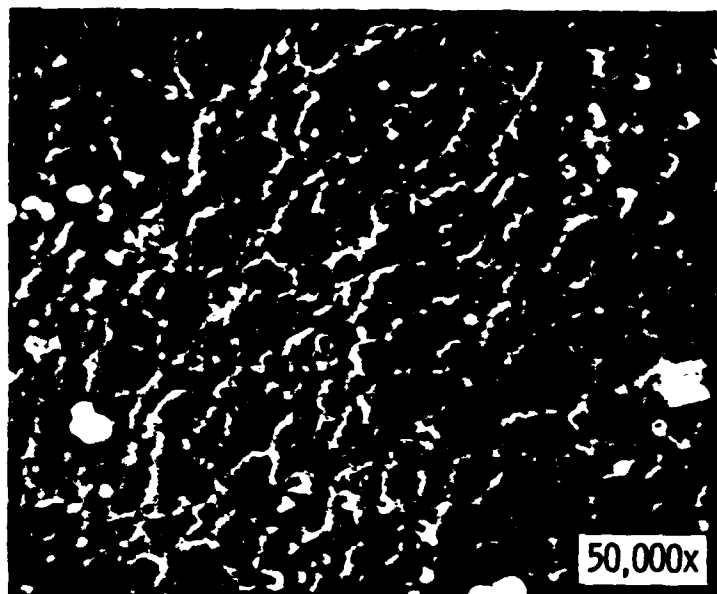
Figure 19. URSEM photomicrograph of thermal oxide film on alloy B showing porosity.
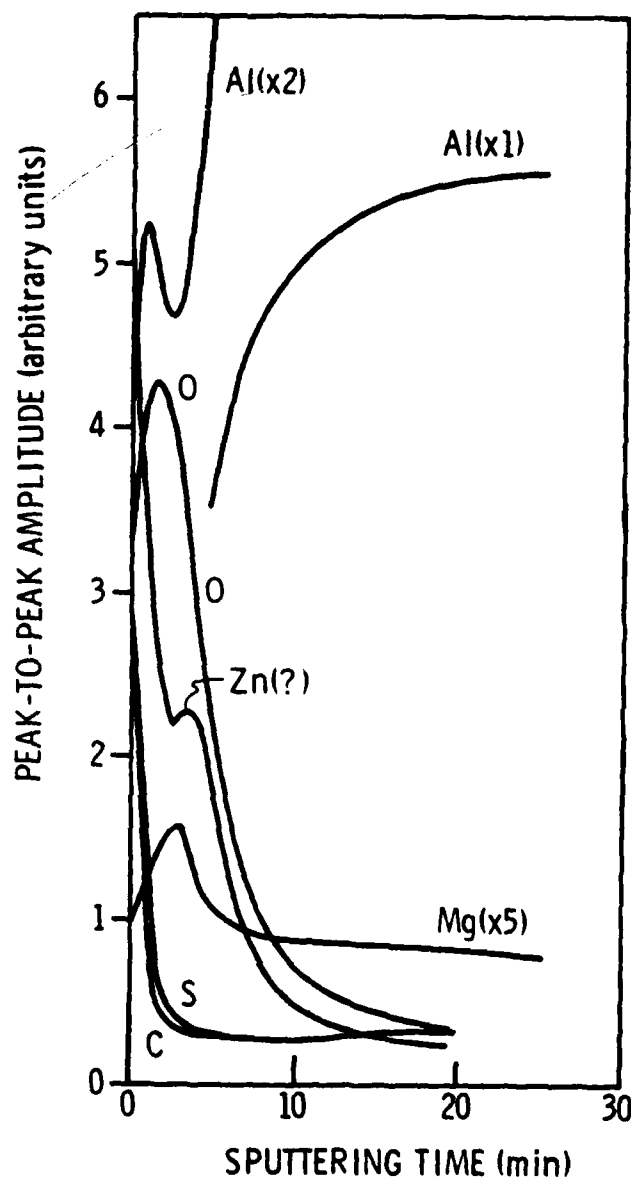
Figure 20. Auger depth profile of naturally-formed oxide on alloy B.

Figure 21. Mudcracking on fracture surface of alloy B.

structure has no relationship to the microstructure of the substrate, and
this is consistent with our findings. That is alloy B has a mean grain size of
15 μm x 9 μm, and the approximate size of the mud cracking feature is 3 μm.
Ultrasonic cleaning, adhesive tape, and several replicating methods have
failed to remove the corrosion product on most specimens. However, the
corrosion product was successfully stripped from a short-time (highly stressed)
specimen of alloy B having a thermal oxide.

The major portion of the fracture path of this specimen clearly is
intergranular, as can be seen in Fig. 22. Secondary cracks often extend into
the bulk of the specimen along grain boundaries as shown in Fig. 23. As stress
corrosion proceeded and the load-bearing section of the specimen was reduced,
the fracture mode switched from an intergranular to a more ductile, transgranular
fracture mode. Figure 24 shows the transition region between these two modes
of fracture. No signs of precipitate dissolution were evident. Figures 22-24
were taken on a SEM; the URSEM will be used in subsequent examinations to more
clearly observe the fracture path.

Figure 22. Region of intergranular fracture at edge of alloy B thermal
specimen. Note that secondary cracks are also intergranular
(1000 X).

Figure 23. Another region of intergranular fracture on same specimen
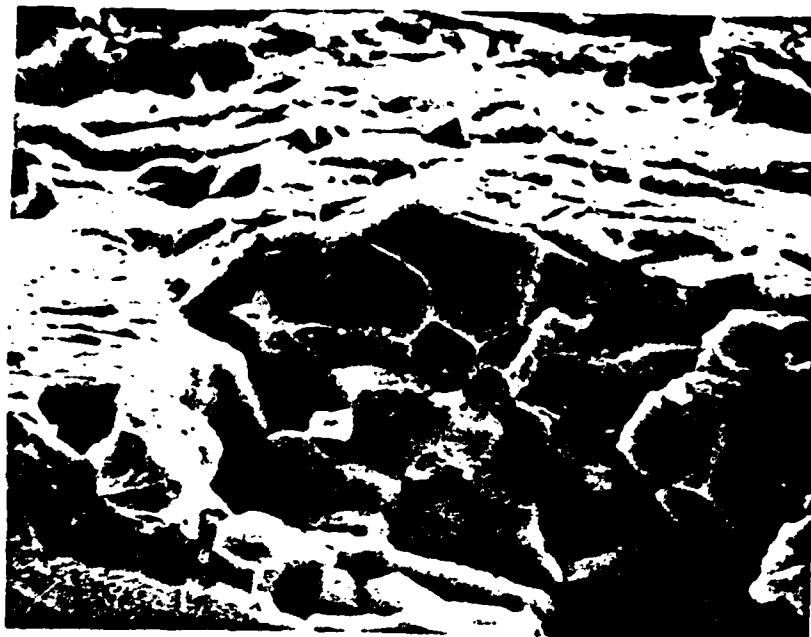as Figure 22 (1000 X).

Figure 24. Transition region between intergranular SCC region and
transgranular, fast fracture region (1000 X).

IV. CONCLUSIONS

1. The original ingots purchased from Metals Specialties Co. were overly porous, which has resulted in excessive scatter in stress-life data of sheet rolled from the ingots. Consequently, several experiments will be repeated on newly obtained, high-purity alloys.

2. Within the limitations imposed by the scatter in the data, it appears that for alloys where the thermal oxide films have been removed, high bulk Mg/Zn has a slight adverse effect on SCC resistance. This is mildly supportive of our view that a Mg-H interaction may be involved in the SCC of Al-Zn-Mg alloys.

3. An oxide stripping procedure has been developed that removes the magnesium-rich oxide film developed during solution treatment and allows formation of a "natural," amorphous alumina film. Preliminary results indicate that alloys with this oxide film may have increased SCC resistance.

4. No great gains in SCC resistance were obtained by interrupted quenching; hence, these experiments were terminated.

ACKNOWLEDGEMENT

REFERENCES

1. A.J. Sedriks, J.A.S. Green, and D.L. Novak: Proc. U.R. Evans Int. Conf. on Localized Corrosion, p. 569, edited by R.W. Staehle, Williamsburg, VA, NACE, 1971.

2. A.J. Sedriks, J.A.S. Green, and D.L. Novak: "On the Chemistry of the Solution at Tips of Stress Corrosion Cracks in Al Alloys," Corrosion NACE, 1971, Vol. 27, No. 5, p. 198.

3. J.A.S. Green and W.G. Montague: "Observations on the Stress Corrosion Cracking of an Al-5% Zn-2.5% Mg Ternary and Various Quaternary Alloys," Corrosion, 1975, Vol. 31, No. 6, p. 206.

4. A.J. Sedriks, J.A.S. Green, and D.L. Novak: "The Influence of Heat Treatment on the Stress Corrosion Susceptibility of a Ternary Al-5.3Zn-2.5Mg Alloy," Metall. Trans., 1973, Vol. 4, p. 1992.

5. E.N. Pugh, J.A.S. Green, and A.J. Sedriks: "Current Understanding of Stress Corrosion Phenomena," March 16, 1969.

6. A.J. Sedriks, J.A.S. Green, and D.L. Novak: "Comparison of the Corrosion and Stress-Corrosion Behavior of a Ternary Al-Zn-Mg Alloy," Metall. Trans., July 1980, Vol. 1, p. 1815.

7. J.A.S. Green, H.W. Hayden, and W.G. Montague: "The Influence of Loading Mode on the Stress Corrosion Susceptibility of Various Alloy/Environment Systems," Effect of Hydrogen on Behavior of Materials, p. 200, edited by A.W. Thompson and I.M. Bernstein, AIME, Philadelphia, PA, 1976.

8. C. St. John and W.W. Gerberich: "The Effect of Loading Mode on Hydrogen Embrittlement," Metall. Trans., 1973, Vol. 4, p. 589.

9. J.C.M. Li, R.A. Oriani, and L.S. Darken: Z. Phys. Chem., 1969, Vol. 49, p. 271.

10. J.K. Tien, A.W. Thompson, I.M. Bernstein, and R.J. Richards: "Hydrogen Transport by Dislocations," Metall. Trans. A., 1976, Vol. 7A, p. 821.

11. R.J. Gest and A.R. Troiano: "Stress Corrosion and Hydrogen Embrittlement in an Aluminum Alloy," Corrosion, 1974, Vol. 30, No. 8, p. 274.

12. L. Montgrain and P.R. Swann: "Electron Microscopy of Hydrogen Embrittlement in a High Purity Al-Zn-Mg Alloy," Hydrogen in Metals, Proc. Int. Conf. on the Effects of Hydrogen on Materials Properties and Selection and Structural Design, p. 575, edited by I.M. Bernstein and A.W. Thompson, ASM, Champion, PA, 1973.

13. R. Alani and P.R. Swann: "Water Vapour Embrittlement and Hydrogen Bubble Formation in Al-Zn-Mg Alloys," Br. Corros. J., 1977, Vol. 12, No. 2, p. 80.

14. M.O. Speidel: "Hydrogen Embrittlement of Aluminum Alloys?" _Hydrogen in Metals_, Proc. Int. Conf. on the Effects of Hydrogen on Materials Properties and Selection and Structural Design, p. 23, edited by I.M. Bernstein and A.W. Thompson, ASM, Champion, PA, 1973.

15. J. Albrecht, A.W. Thompson, and I.M. Bernstein, "The Role of Micro-structure in Hydrogen Assisted Fracture of 7075 Aluminum," _Metall. Trans. A_, 1979, Vol. 10A, p. 1759.

16. G.M. Scamans, R. Alani, and P.R. Swann: "Pre-exposure Embrittlement and Stress Corrosion Failure in Al-Zn-Mg Alloys," _Corros. Sci._, 1976, Vol. 16, No. 7, p. 443.

17. J. Maloney: Ph.D. Thesis, Carnegie Mellon Institute, 1980.

18. J. Maloney: Presentation at AIME Meeting in Las Vegas, February 1980.

19. A. Csanády and D. Martin: "Stress Corrosion Behavior of Al-Zn-Mg Alloys Based on Microchemical Surface Reactions," _J. Mater. Sci._, 1979, Vol. 14, p. 2289.

20. J.A.S. Green, R.K. Viswanadham, T.S. Sun, and W.G. Montague: "Grain Boundary Segregation and Stress Corrosion Cracking of Aluminum Alloys," _Corrosion/77_, _Proc. Int. Corrosion Forum_, p. 17/1, San Francisco, CA, 1977.

21. R.K. Viswanadham, T.S. Sun, and J.A.S. Green: "Grain Boundary Segrega-tion in Al-Zn-Mg Alloys -- Implications to Stress Corrosion Cracking," _Metall. Trans. A_, 1980, Vol. 11A, p. 85.

22. R.K. Viswanadham, T.S. Sun, and J.A.S. Green: "Auger Electron Spectro-scopy Studies of Oxide Films on Al-Zn-Mg Alloys," accepted for publica-tion in _Corrosion_.

23. J.M. Chen, T.S. Sun, R.K. Viswanadham, and J.A.S. Green: "Grain Boundary Segregation of an Al-Zn-Mg Ternary Alloy," _Metall. Trans. A_, 1977, Vol. 8A, p. 1935.

24. P. Doig and A.W. Edington: "Stress Corrosion Susceptibility of As-Quenched Al-5.9 wt.% Zn-3.2 wt.% Mg Alloys," _Br. Corros. J._ (Quarterly), 1974, Vol. 9, No. 4, p. 220.

25. T.S. Sun, J.M. Chen, R.K. Viswanadham, and J.A.S. Green: "Plasmon-Loss Satellites in Auger Spectra of Alloy Surfaces," _Appl. Phys. Lett._, 1977, Vol. 31, No. 9, p. 580.

26. F. Degréve: "New Methods for Determining Hydrogen Content in Aluminum and Its Alloys," _J. Metals_, 1975, Vol. 27, No. 3, p. 21.

27. E. Hidvégi and E. Kovács-Cserényi: "Study of the Loss of Magnesium in an Al-Mg-Si Alloy," _Mat. Sci. and Eng._, 1977, Vol. 27, p. 39.

28. P.D. Hess: "An Empirical Equation for Calculating Solubility of Hydrogen in Molten Aluminum Alloys," _Light Metals (AIME)_, 1974, Vol. 2, p. 591.

29. T.S. Sun, J.M. Chen, R.K. Viswanadham, and J.A.S. Green: "Surface Activities of Mg in Aluminum Alloys," J. Vac. Sci. Technol., 1979, Vol. 16, No. 2, p. 668.

30. K. Asano, M. Abe, and A. Fugiwara: "Nucleation of Precipitates in Al-Zn-Mg Alloys," Mater. Sci. Eng., 1976, Vol. 22, p. 61.

31. A.J. Sedriks, J.A.S. Green, and D.L. Novak: "The Influence of Heat Treatment on the Stress Corrosion Susceptibility of a Ternary Al-5.3 Pct. Zn-2.5 Pct. Mg Alloy," Metall. Trans., 1973, Vol. 4, p. 1992.

32. P.R. Sperry and M.H. Bankard: ASM Metals Handbook, Vol. 8, 8th edition, p. 120, ASM Publication, Metals Park, OH, 1973.

33. H.W. Eichner and W.E. Schowalter: Forest Products Laboratory Report No. 1813, 1950.

34. J.D. Venables, D.K. McNamara, T.S. Sun, B. Ditchek, J.M. Chen, and R.L. Hopping: Proc. Structural Adhesives and Bonding Conf., p. 12, Technology Conferences Associates, El Segundo, CA, 1979.

35. J.D. Venables, D.K. McNamara, J.M. Chen, T.S. Sun, and R.L. Hopping: Appl. Surf. Sci., 1979, Vol. 3, p. 88.

36. B.F. Brown: "Stress Corrosion Cracking Control Measures," U.S. Dept. of Commerce, NBS Monograph 156, 1977.